Report for the Dr Eduard Gübelin Research Scholarship 2016

awarded by

The Dr Eduard Gübelin Association
for Research & Identification of Precious Stones

DR. EDUARD GÜBELIN
ASSOCIATION

About the project

THE OPAL INSTABILITY ENIGMA: A KEY FROM WATER AND MICROSTRUCTURE

By Boris Chauviré

May 2018

TABLE OF CONTENTS

1. EXECUTIVE SUMMARY 1
2. INTRODUCTION 3
   2.1 Proposed processes 4
      2.1.1 Drying shrinkage 4
      2.1.2 Internal water pressure 5
      2.1.3 Light scattering 5
   2.2 Characterization methods 6
3. SAMPLES 7
4. METHODS 9
   4.1 Gas adsorption 9
   4.2 Thermogravimetric Analysis 9
   4.3 Thermoporosimetry (Differential Scanning Calorimetry) 9
   4.4 Raman Spectroscopy 9
5. RESULTS 10
   5.1 Gas adsorption 10
   5.2 Thermogravimetric Analysis 10
   5.3 Thermoporosimetry (Differential Scanning Calorimetry) 11
      5.3.1 Crystallizable water content 11
      5.3.2 Water-filled pores size 12
      5.3.3 Pore size distribution (PSD) 13
   5.4 Raman Spectroscopy 14
      5.4.1 Cracking of fresh samples 14
      5.4.2 Cracking of old samples 15
6. DISCUSSION 16
   6.1 Incorporation of water in opal 16
      6.1.1 Water speciation 16
      6.1.2 Water-filled porosity 17
   6.2 Reactions during heating dehydration 17
   6.3 Cracking origin? 18
      6.3.1 Internal water pressure 18
      6.3.2 Drying shrinkage 19
7. CONCLUSION 20
8. REFERENCES 21

1. EXECUTIVE SUMMARY

Gem opal has always held many mysteries. The origin of the play of colour has intrigued scientists since antiquity. The advance of the characterisation method allowed identification of the origin of this phenomenon during the 60s (Jones et al., 1964; Darragh & Sanders, 1965). However, opal still keeps the secrets of its instability. Indeed, opal may crack or change in transparency after extraction. Opal destabilization has been classified into 2 main types: cracking, and whitening (Pearson, 1985; Fritsch et al., 1999; Aguilar-Reyes, 2004; Rondeau et al., 2011). The first is due to the development and/or the extension of a network of micro-fractures that can damage the integrity of the stone; the second is the decrease of transparency due to light scattering, resulting in a whitish, milky appearance. Besides the loss of commercial value (cracking opal may become totally worthless), opal instability implies a significant loss of cultural and natural heritage.

The aim of the project was to provide novel data to better understand the process(es) involved in the destabilization. Three models are proposed to explain the destabilization: drying shrinkage, internal water pressure, and light scattering. Drying shrinkage is the decrease of volume during the loss of water. It is well studied in silica gel (Brinker & Scherer, 1990; Scherer, 1992b, 1997; Smith et al., 1995), which has been suggested as the precursor for opal precipitation (Darragh et al., 1976; Iler, 1979). An internal water pressure occurs if the pressure produced by water enclosed in closed porosity is greater than the resistance of the material. The last model - light scattering - may only explain the whitening, with a scattering of light due to the creation of an area of different optical characteristics due to the loss of water from porosity.

In order to provide data on the destabilization, a comprehensive set of characteristic opal has been used, with “old samples” - that is samples extracted several years before analysis and preserved in the atmosphere - and “fresh samples”, extracted recently and preserved in water until analysis. The cracking and whitening of old samples has been identified with heating experiments (Chauviré, 2015). The total water content and the behaviour of water release during heating has been assessed using thermogravimetric analysis (TGA). Differential Scanning Calorimetry (DSC) provides the proportion of free molecular water in opal, and the pore size enclosing this water species. Moreover, the stress during cracking has been investigated by examining the samples between cross-polars and by Raman spectroscopy.

The TGA can be used to classify the opals according to their behaviour. We identify opals that dehydrate gradually, opals that lose water between 300°C and 600°C, and opals that release water at “low” temperatures (less than 300°C). DSC analysis indicates that up to 45 % of the total water (measured by TGA) is present as free water, and this water species resides in nanometric pores. The stress characterization (by polarized light and Raman spectroscopy) determined that old and fresh samples react differently. Fresh samples exhibit anisotropic features and a shift in the Raman mode, characteristic of stress in the material, even after cracking. By contrast, old samples do not show any stress during or after the cracking.

All the data point toward a difference between freshly-extracted opals and ancient opals. As any other material, there is a range of conditions outside which opals are no longer resistant. Using the model of Linear Elastic Fracture Mechanism, and the parameter measures in the literature on natural opals (Thomas et al., 2008), we calculate that the critical pressure (required to induce cracking) ranges from 400 MPa to 13.5 GPa (according to the crack length). The pressure induced by water enclosed in opals during heating may reach several hundreds of MPa, and may explain the cracking of old samples that dehydrate at high temperatures (over 300°C). This process is consistent for some samples

with a TGA analysis showing a dehydration after cracking (indicating water enclosed in closed porosity), relatively rich in free water (from DSC), and no remaining stress after cracking (from polarized light and Raman spectroscopy). By contrast, cracking of fresh samples is consistent with drying shrinkage. Models of drying stress estimate a pressure sufficient to crack opals. In addition, this is consistent with the stress remaining after cracking.

The project has provided novel data to understand the incorporation of water in opals, and the process of dehydration in opals. It appears that the process of destabilization depends on the method employed to preserve samples. However, further investigation is required to elaborate an efficient protocol of diagnosis.

2. INTRODUCTION

Gem opals have acquired an unquestionable place in the gem trade, with a long cultural history around the world. However, their striking beauty may be altered by an as yet unexplained phenomenon: opal may “craze” or degrade with time. According to current knowledge, opal destabilization is associated with changes in its structure at the micro- and nano-scopic scale, and with loss of water. However, the details of these processes remain unknown, which prevents the development of prophylactic mitigation strategies. Besides the decrease in commercial value, opal instability implies a significant loss of cultural and natural heritage. Opal extraction is often performed by economically-fragile communities for which the money earned through opal mining profoundly impacts the local economic and social outlook. The present project intends to provide novel data to understand which process(es) are involved in the destabilization of opal.

Opal is a variety of amorphous silica (SiO2.nH2O) that may display striking and uniquely-patterned play-of-color, thus attracting high demand prices on the gem market. The origin of the play-of-color was explained during the 60s through observation of the regular network of nanometric silica spheres (Jones et al., 1964; Sanders, 1964). However, opals may suffer a change in transparency or start cracking once they have been removed from the ground. Opal destabilization has been described and categorized into 2 main types: cracking and whitening (Pearson, 1985; Fritsch et al., 1999; Aguilar-Reyes, 2004; Rondeau et al., 2011). The first is the development and/or the extension of a network of micro-fractures that can extend into and damage the body of the stone (Figure 1, left); the second is the decrease of transparency due to light scattering, resulting in a whitish, milky appearance (Figure 1, right). Curiously, few studies have explored opal stability, even though it impacts much of the world’s opal.

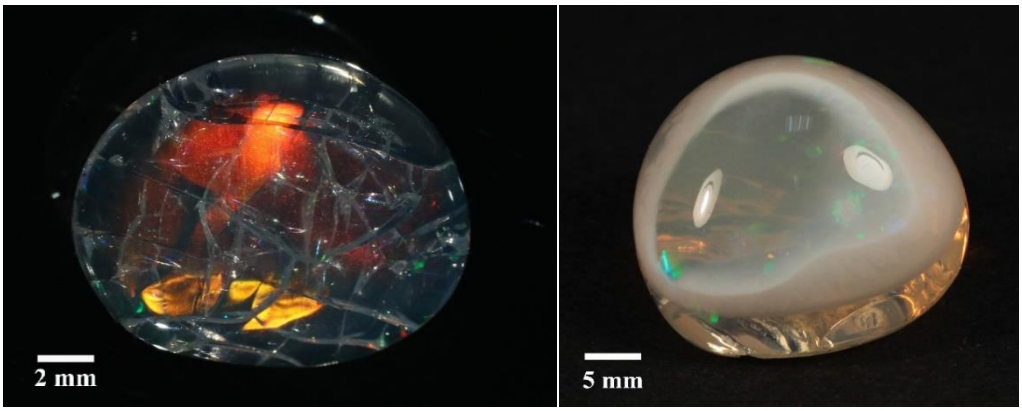

Figure 1 : Opals from Wegel Tena (Ethiopia) developing cracking (left) and whitening (right). Photographs by B. Rondeau.

Cracking is generally first observed at the surface of the sample, and may develop through the stone over time (Rondeau et al., 2011). Pearson (1985) is the first and only study that clearly establishes a link between opal cracking and the loss of water, but this study is restricted to a limited set of Australian opals. Some studies focus on the stability of opal from specific deposits without explaining the process (Johnson et al., 1996; Smith, 1988; respectively on opals from Mezezo - Ethiopia- and Oregon –USA). Thermomechanical behaviours of opal have shown an expansion followed by a contraction of the materials (Jones & Segnit, 1969; Frischat et al., 1989; Brown et al., 2002). A general correlation has been found between the temperature of transition of mechanical behaviour and the temperature of maximum dehydroxylation (measured by thermogravimetric

analysis; Brown et al., 2002), demonstrating the correlation between the loss of water and changes in the microstructure. However, these studies are restricted to Australian opals-A.

Whitening manifests as more translucent regions (as bands or "eggs") following the outside contour of the sample, and sometimes as a shell with a more transparent region occurring within (Aguilar-Reyes, 2004; Rondeau et al., 2011). Few studies have focused on the comparison between the whitened (destabilized) regions and the stable regions of opals. Aguilar-Reyes (2004) and Paris et al. (2007) demonstrate, using X-ray diffraction (XRD), Raman spectroscopy and nuclear magnetic resonance (NMR), that no structural differences in the silica framework can be found between whitened and stable regions. Nevertheless, Aguilar-Reyes (2004) observes, at microscopic scale, that opals undergo changes in their micro-structure. First, the whitened regions have a specific area (proxy of the porosity, measured by gas adsorption and BET method) 1 to 35 times higher than stable regions. Secondly, Aguilar-Reyes (2004) observes, by scanning electronic microscope, either the appearance of holes of 200-1000 nm in diameter, or a change in the compactness of the material. She concludes that the whitening is associated with an opening of the porosity of the opal, without changes in the structure of the silica itself. The porosity will enhance light scattering in the materials, and thus leads to the whitening.

2.1 Proposed processes

The studies cited above restrict the processes that might possibly be involved in destabilization. It is well-established that the loss of water is correlated to the destabilization, for both whitening and cracking. Opal contains two types of water species : molecular water (trapped in silica in existing porosity) and hydroxyl groups (silanol groups, Si-OH). The destabilization of opal appears to be associated with the loss of molecular water (Pearson, 1985; Brown et al., 2002; Aguilar-Reyes, 2004; Paris et al., 2007). Several processes are suggested in the present project: drying shrinkage, internal water pressure, and light scattering from porosity.

2.1.1 Drying shrinkage

The drying of silica gel, regularly proposed as the precursor of opal (Darragh et al., 1976; Iler, 1979), has been well documented (Brinker & Scherer, 1990; Scherer, 1992b, 1997; Smith et al., 1995; Thiery et al., 2016). A gel can be roughly defined as a solid diluted in a liquid. The drying of a gel will result in a solid material. Several stages of drying have been identified during the loss of liquid from the gel. The first phase takes place when the shrinkage of the gel is equal to the volume of the liquid lost. The evaporation of the liquid (driven by the difference in vapour pressure inside the gel and in the atmosphere) reduces the volume of liquid in the gel. The meniscus forms at the surface of contact between the liquid and the vapour phase (the evaporation limit) and induces a tensile stress on the rim of the solid material, bringing them closer. This step ends when the stiffness of the materials cannot deform efficiently to adapt to the stress induced. In particulate gel (gel constituted by particles of solids, which is the case with the precursor of opal), shrinkage may continue after particles come into contact, until particles rearrange into a closer-packed network. At this so-called critical point, shrinkage stops and further evaporation drives the meniscus into the body of the gel. The capillary force (induced by the meniscus of liquid in the porosity) is maximum at this point. The tension at the drying surface is dependent on the interfacial energy between liquid and vapour, the contact angle between the liquid and the solid (a proxy of the hydrophobicity of the material), and the

pore radius. The rigidity of the solid and the capillary pressure are the main parameters controlling the cracking process and the propagation of the cracks (all details may be found in the following reviews: Brinker and Scherer, 1990; George W. Scherer, 1992; Smith et al., 1995). The liquid/vapour interface recedes into the porosity of the material. Isolated pockets of filled pores may remain near the interface and enhance the scattering of light, lowering the transparency of the material. The transition surface between the fully-saturated and the dried regions has been observed to form an opaque to translucent limit (Scherer, 1992b; Hench, 1998).

As observed during the destabilization of opals, cracking of a silica gel occurs preferentially at the surface, where the interface starts to enter into the material. Moreover, the "white egg" documented in some opals, with an opaque white shell around a translucent core following the outside contour of the sample (Aguilar-Reyes, 2004; Rondeau et al., 2011) appears consistent with the drying of a silica gel. Consequently, in this model, unstable opals are immature silica gel. Several studies have proposed various methods of predicting and/or avoiding cracking, and these may be applied to opal (Kistler, 1931; Zarzycki et al., 1982; Phalippou et al., 1990; Scherer, 1992b; Smith et al., 1995).

2.1.2 Internal water pressure

Opals contain water molecules in silica cages. The incorporation of water during the precipitation of opal occurs during the drying of a silica gel that may enclose water in porosity (see subsection above). The conditions of opal precipitation, and subsequently the incorporation of water in opal, are consistent with a higher vapour pressure (required for the formation of gel, Darragh et al., 1976; Iler, 1979) than that of the actual atmosphere. The stone remains in equilibrium with the ground vapour pressure. The extraction of the material exposes the opal to the lower atmospheric vapour pressure (compared to that in the ground). Water enclosed in porosities exerts a pressure inside the opal, and may lead to a cracking of the silica framework. Another way of increasing the internal pressure induced by water in inclusions is heating. Indeed, fluid expansion within pores as a result of thermal treatment exerts a pressure on the host mineral, thus inducing cracking (Wanamaker et al., 1990; Vityk & Bodnar, 1995; Hansteen & Klugel, 2008).

For this model, water molecules must be enclosed within a low-connected porosity. Indeed, a connected porosity will enhance the release of water under pressure, and thus avoid the cracking usually caused by this process. Moreover, in this case, the opal is extracted from a host-rock with a high vapour pressure, implying that origin may be a significant factor. However, it appears that all sources of opal are subject to the destabilization (Rondeau et al., 2011).

2.1.3 Light scattering

Light scattering is a well-known phenomenon where light traverses a transparent medium and encounters diffusers with a different refractive index (e.g. small particles: Born et al., 1999). According to the size of the particle, several type of scattering may occur. If the size of the particle is < 0.1 of the wavelength of the light, we observe a Rayleigh scattering, whereas Mie scattering is the main phenomenon for larger particles (up to 10 times the wavelength). Both Rayleigh and Mie scatterings are elastic, meaning that the energy (and thus the wavelength) of the light before and after scattering is similar. The main difference is the wavelength dependency of the scattering. Rayleigh scattering is a function of wavelength, favouring the scattering of low wavelengths (according to a λ^{-4} relation – with λ as the wavelength - explaining the blue colour of the sky due to air molecules). The

blue appearance of opalescent materials (including opal) is commonly attributed to the Rayleigh scattering (Lockwood, 2015). For larger diffusers (more than 10 times the wavelength), geometric scattering, which results from multiple reflections on the surface of each "particle", is the main scattering phenomenon.

This model may explain the whitening but not the cracking of opal. The whitening is assumed to result from scattering in the existing, previously dried, porosity of opal. Before the dehydration, the water enclosed in the porosity prevents the scattering (due to the closer refractive index of opal compared to air - n_{water} = 1.33, n_{opal} = 1.37-1.47 (Des Cloizeaux, 1862; Lacroix, 1896; Cassedanne & Cassedanne, 1975; Gauthier et al., 2004, n_{air} = 1). Indeed, the replacement of water by air in the porosity will enhance the scattering, in proportion to the size of the porosity. This explains the behaviour of hydrophane opal, which becomes transparent when immersed in water, and becomes opaque again during drying (Figure 2).

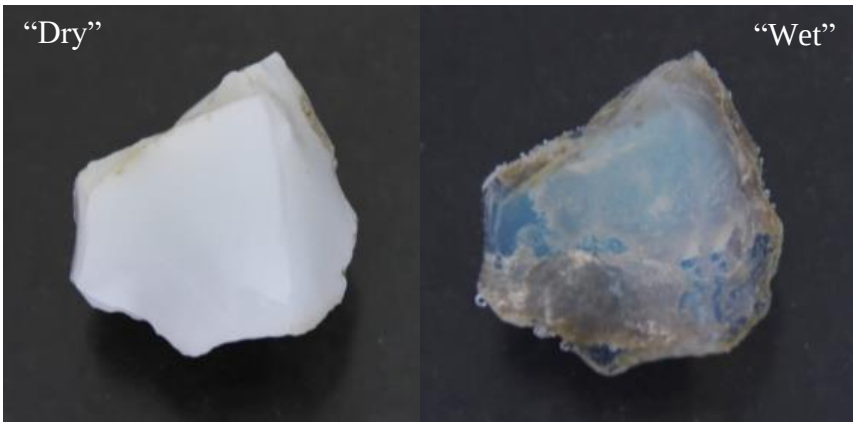

Figure 2: Same sample before and after immersion in water. We note that the transparency increases drastically after addition of water. The appearance of the blue hue is characteristic of Rayleigh scattering.

2.2 Characterization methods

In order to identify the process involved in the destabilization, we performed several analyses to constrain the hydration and the behaviour of opal during the dehydration. The hydration of opal was characterized through thermogravimetric analysis (TGA) and thermoporosimetry (based on differential scanning calorimetry, DSC). TGA measures the total water content of each sample, and the development of thermoporosimetry, based on DSC, determines the pore size and the amount of crystallizable water (free water) using the depression of the melting (or crystallization) temperature of the liquid confined in pores (Brun et al., 1977; Ishikiriyama & Todoki, 1995; Landry, 2005; Thomas et al., 2013). Gas adsorption was set up to characterize the porosity of the samples. To define the stress during the loss of water, we performed Raman spectroscopy with a heating cell to accelerate the dehydration and the subsequent destabilization. Indeed, Raman modes shift in frequencies with increasing stress (Tallant et al., 1988; Perriot et al., 2006; Malchow et al., 2015).

Several collaborators participated in this project. B. Rondeau, assistant professor at the University of Nantes, who supervised Valentin Mollé during his master's thesis on the characterization of cracking by Raman spectroscopy. Paul Thomas, professor at the University of Technology, Sydney, who greatly helped with the DSC and TGA analyses (acquisition and interpretation).

3. SAMPLES

During this project, 24 opal specimens were analysed, 3 of which were opal-A and 21 of which were opal-CT from various origins (mainly from Mexico and Ethiopia for opal-CT; details in Table 1 below). More details about the geological context and structure are outlined in Chauviré et al. (2017). Among them, 19 samples were either from a gem collection (from CRG, Centre de Recherche Gemmologique), or directly collected at the mining site (especially for samples from Wegel Tena or Jalisco). The 5 remaining samples (noted with a * in Table 1 below) were collected at the mining sites and preserved in water to avoid dehydration (hereafter called "fresh samples"), compared to other samples, which were exposed to the atmosphere (hereafter called "old samples"). These samples were collected by Selam Dagnachew (an MSc student at the University of Addis Abeba, supervised by Dereje Ayalew), at the mine of Koke Woha (noted KOK, location available in Chauviré et al., 2017b), Anset and Chegen (noted AN et CH, located at 11°33'24.7"N/39°9'8.3"E ; 11°42'54.2"N/39°17'7.1"E respectively). A detailed description can be found in Mollé (2017).

Variety	Sample	Geographic Origin
Opal-A	**785**	Honduras
	86.2	Kashau, Slovakia
	1040	Coober Pedy, South Australia, Australia
Opal-CT	**928**	Mali
	1085	"New Maternal", Argentina
	1545	Unknown
	1548	Fougères, Brittany, France
	1543a	San Martin, Jalisco, Mexico
	1543b	
	1552b	
	1552d	
	43l	Humboldt County, USA
	521	Mezezo, Ethiopia
	1551	
	YM12	
	208	Wegel Tena, Ethiopia
	FT1111	
	VTB	
	WT86	
	KOK01*	
	KOK04*	
	KOK05*	
	CH01*	
	AN02*	

Table 1: Opal samples used in this project. Samples noted with a * were directly collected at mines and preserved in water until analysis.

All samples were structurally characterized by Raman spectroscopy in Chauviré et al. (2017a) and Mollé (2017). The 19 old samples were also analysed using infrared spectroscopy in Chauviré et al. (2017a). Moreover, the dehydration during heating of these samples was investigated by infrared spectroscopy (Chauviré, 2015). During heating experiments, the behaviour (cracking and whitening) of each sample was observed (Table 2). The heating experiments consisted in successive heating steps (room temperature, 150, 300, 350, 400, 450, 500, 550, 600, 700, 850, 1000°C) in an oven (with no purge) and cooling in sealed cells to analyse by infrared spectroscopy.

Variety	Sample	Behaviour during heating	
		Cracking at	Whitening at
Opal-A	**785**		300 °C
	86.2		300 °C
	1040	300 °C	
Opal-CT	**928**	RESIST	
	1085		
	1545	RESIST	
	1548	300 °C	
	1543a	300 °C	
	1543b	300 °C	
	1552b	300 °C	500 °C
	1552d	300 °C	500 °C
	43l		700 °C
	521	300 °C	
	1551		500-850 °C
	YM12		850-1000 °C
	208		350 °C
	FT1111	RESIST	
	VTB	RESIST	
	WT86		1000 °C

Table 2: Temperature of cracking and/or whitening during the heating experiments from Chauviré (2015)

The 5 fresh samples were cut into two pieces to compare the behaviour during heating and when exposed to the atmosphere (reference sample).

4. METHODS

4.1 Gas adsorption

Nitrogen adsorption-desorption measurements were performed on a Gemini VII 2390 surface area analyser (Micromeritics), at the University of Technology, Sydney. Samples were cut and/or broken into pieces of hundreds of milligrams (from 200 to 600 mg) and degassed at 40°C and under vacuum for 2 to 4 days to remove superficial water and ensure access to the porosity.

4.2 Thermogravimetric Analysis

Thermogravimetric analyses were performed on 19 old samples. Total water content was measured using thermogravimetric analysis (TGA), with a Setaram Setsy 16/18 instrument, at the School of Mathematical and Physical Science, University of Technology, Sydney. Pieces of each opal specimen (from 29.5 to 83.6 mg) were placed in 130 µL platinum pans (4,5 mm diameter and 8 mm height) with platinum caps on the crucible (to avoid the loss of material during the possible cracking). Two sets of analyses were performed: on 5 samples, water loss was measured from 20 to 1100°C with a heating rate of 2°C.min^{-1} on 3 pieces of the same sample; and for the 14 remaining samples, measurements were carried out from 20 to 1000°C with a heating rate of 10 °C.min^{-1} by single piece. Temperature calibration was carried out using the melting points of high purity zinc, lead, aluminium, copper and gold. As the furnace is a vertical furnace, a baseline calibration was carried out using the experimental conditions with the empty crucibles in place. The baseline was subtracted from the experimental data using a point to point basis.

4.3 Thermoporosimetry (Differential Scanning Calorimetry)

Nineteen opal samples were prepared for DSC analysis by breaking and/or cutting small pieces (from 11.1 to 29.2 mg) of each specimen which were then sealed in a TZero aluminium pan and lid. DSC analyses were performed using a TA Instrument Q2000 fitted with the RCS90 refrigerated cooling system. Samples were cycled between -85 and 30 °C with several isothermal steps for equilibration. The DSC analysis were not calibrated for cooling experiments, thus we focused exclusively on heating steps. All the cooling ramps were carried out at 5°C.min^{-1} and heating steps were performed at 2 °C.min^{-1}. Lower heating rates were tried, but noise prevented its value for relevant experiments. A dry air purge was carried out with a flow rate of 50 mL.min^{-1}.

4.4 Raman Spectroscopy

Eight samples (1548, 1552a, 1543b and the 5 samples preserved in water) were prepared as polished thin sections from 160 µm to 2 mm, depending on the fragility of the sample. Rama spectra were acquired using a LabRam HR Evolution (Horiba Scientific) equipped with a 532 nm Ar-ion laser for excitation with a power of 100 mW. Each spectrum was an accumulation of 25 seconds to 1 minute with a resolution of 0.8 cm^{-1} (for 1548, 1552a, 1543b) and 3 cm^{-1} for the 5 fresh samples. The 5 fresh samples preserved in water were analysed by Valentin Mollé, an MSc student at the University of Nantes, supervised by B. Rondeau. Spectra were acquired at room temperature, 150°C and 300°C using a Linkam heating stage adapted to the Raman spectroscope. The heating steps were chosen following the heating experiments in Chauviré (2015). Furthermore, stress were also observed using microscope with cross-polar (polarized light).

5. RESULTS

5.1 Gas adsorption

Within the project, the gas adsorption analyses were not conclusive for the majority of the samples presented here. Indeed, the instrument required a large specific area to be accurately quantified (more than 10 m²/g), thus, for a sample with a limited porosity, it required a larger quantity of sample material than we could provide. Only the 2 most porous samples (VTB and WT86) provided satisfactory results. VTB and WT86 have a surface area of 121±0.3 m²/g and 12±0.2 m²/g respectively.

5.2 Thermogravimetric Analysis

Total water content of the analysed opal ranges from 2.9 to 18.1 wt% (details in Table 3 below). TGA also provides interesting results concerning the hydration behaviour of opal during increases in temperature. Eleven samples (785, 86.2, 1040, 928, 1085, 1545, 1548, 1543a, 1543b, 1552b, 1552d) show no loss of water until 200-400 °C, and a significant dehydration thereafter (sample 1543b in Figure 3). For these samples, up to 90% of the dehydration occurs between 300°C and 700°C. Six samples (208, FT1111, VTB, WT86, 521, YM12) lost most of their water between room temperature and 300°C (sample WT86 in Figure 3). The 2 remaining samples (1551 and 43l) lost their water progressively until 600 or 900°C (sample 1551 in Figure 3).

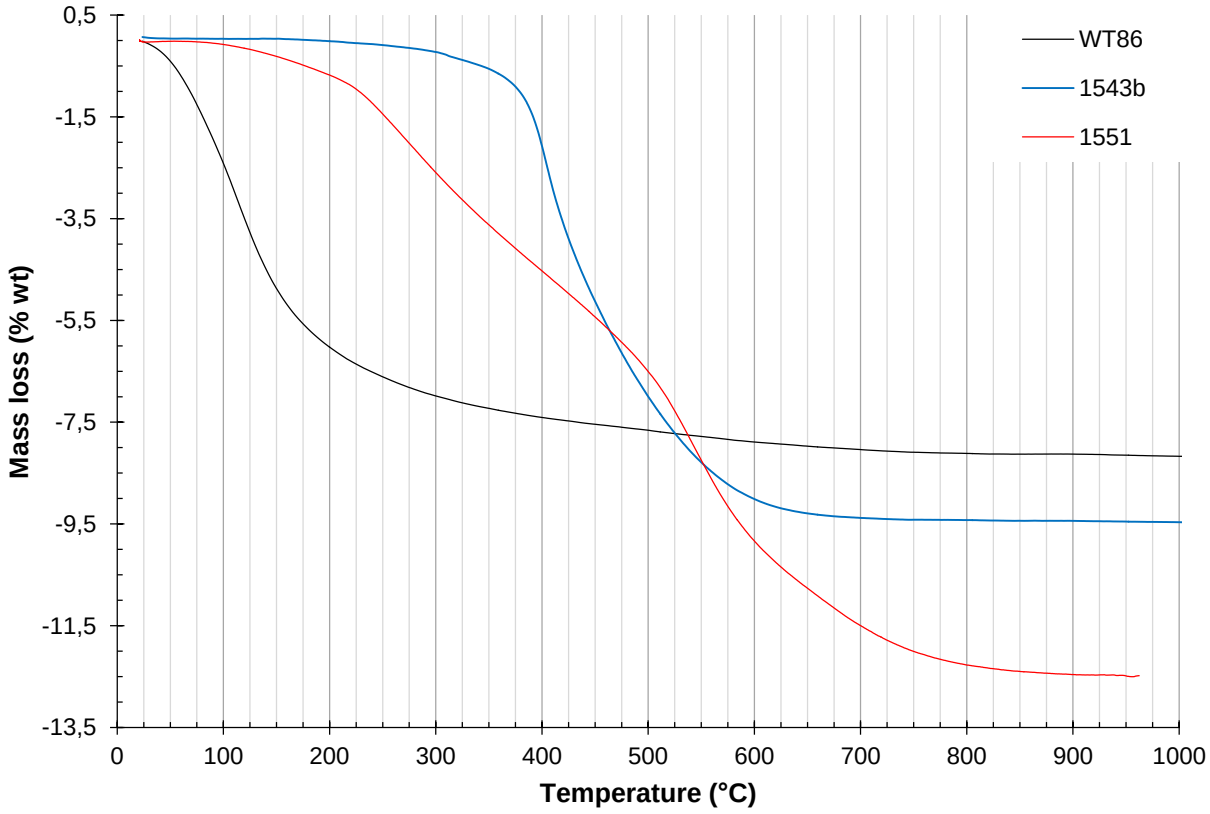

Figure 3: TGA curves of representatives samples of each behaviour.

Sample	Water content (% wt)	Sample	Water content (% wt)
785	4.4	**1552d**	8.5
86.2	4.2	**43l**	2.9
1040	7.3	**208**	18.1
928	2.6	**FT1111**	12.0
1085	6.6	**VTB**	12.3
1545	6.3	**WT86**	8.1
1548	9.5	**521**	8.1
1543a	8.9	**1551**	8.7
1543b	9.3	**YM12**	11.2
1552b	8.6		

Table 3: Water content measured in our sample by TGA.

5.3 Thermoporosimetry (Differential Scanning Calorimetry)

5.3.1 Crystallizable water content

All the heating ramps of the DSC curves are presented in Figure 4. During the heating ramp, the water enclosed in a pore will melt at a temperature related to the size of the pore containing the water, and the area of melting peak is correlated to the amount of molecular water crystallized in the micro-structure (not adsorbed on the opal's inner surface). Consequently, by assuming that the melting temperature of water is independent of the pore size (334 $J.g^{-1}$), we calculate the proportion of crystallisable water in opals (listed in Table 4) that range from 0.1 to 4.3 % weight. No correlations with structure (opal-A and opal-CT) are emphasized.

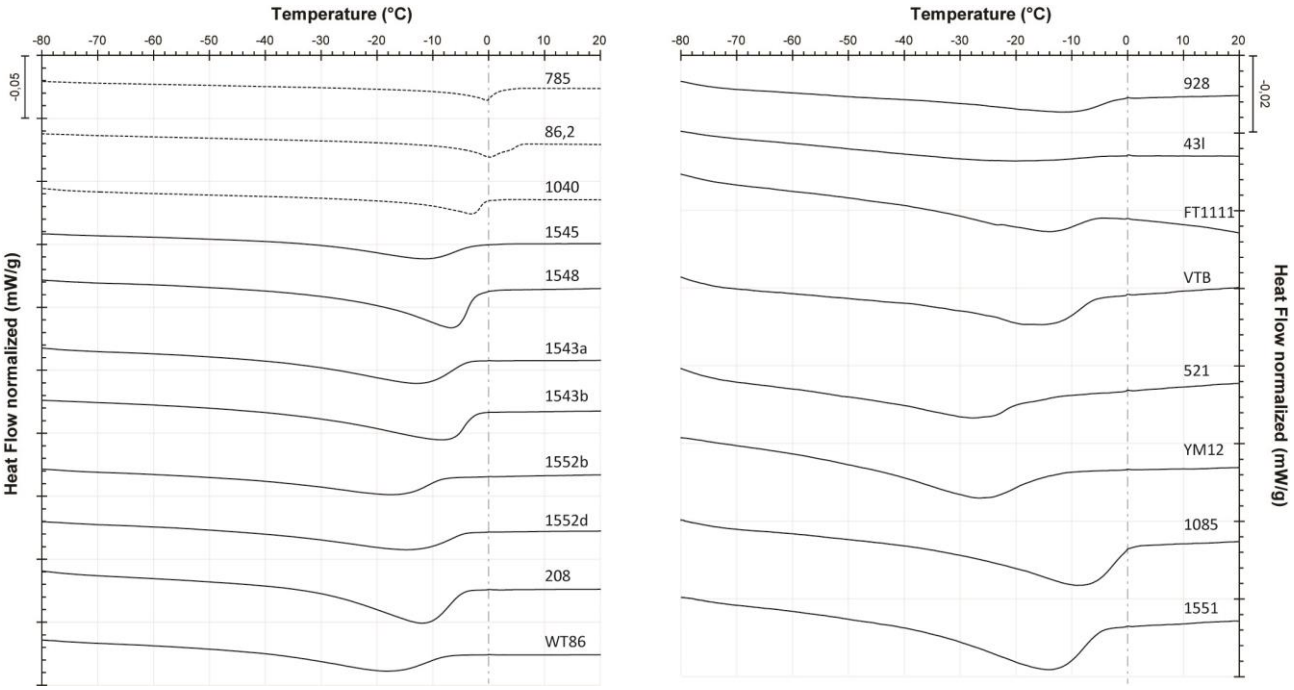

Figure 4: DSC curves of the samples used in this project.

Sample	Peak area (J.g)	Crystallisable water (% wt)	Sample	Peak area (J.g)	Crystallisable water (% wt)
785	2.0	0.6	**1552d**	8.2	2.5
86.2	2.9	0.9	**43l**	0.3	0.1
1040	3.2	1.0	**208**	11.9	3.6
928	0.9	0.3	**FT1111**	2.9	0.9
1085	5.5	1.6	**VTB**	2.2	0.7
1545	6.7	2.0	**WT86**	7.5	2.2
1548	14.5	4.3	**521**	1.4	0.4
1543a	10.2	3.1	**1551**	5.5	1.6
1543b	12.3	3.7	**YM12**	3.4	1.0
1552b	7.2	2.2			

Table 4: Melting peak area from the DSC curves and the calculated proportion of crystallisable water.

5.3.2 Water-filled pores size

Onset temperature (defined as the temperature of intersection between the extrapolated initial base line and the tangent or line through the leading edge of the peak) ranges from -48.1 and -5.6°C, with opal-A having the lower onset temperature (-13.5 to -5.6°C) compared to opal-CT (-48.1 to -18.1°C). These results are consistent with Thomas et al. (2013) (opal-A -7 Australian opals analysed with onset temperature from -15 to -5°C- and opal-CT - one Mexican and one Australian, respectively -32 and -39°C). The empirical equation from Landry (2005) converts the onset temperature on melting peak to the radius of pores containing crystallizable water :

$$r(nm) = -\frac{19.082}{\Delta T + 0.1207} + \delta_m$$

Where r is the radius of crystallizable water-filled pores in nanometres, ΔT is the difference between the onset temperature of the melting peak and the onset temperature of bulk water melting peak (occurring at 0°C), and δ_m is the thickness of non-melting water molecules adsorbed at the surface (1.12 nm; Brun et al., 1977; Landry, 2005). The calculated radii are listed in Table 5. Based on onset temperature alone, opal-A have larger crystallisable water-filled pores (between 2.55 and 4.54) than opal-CT (less than 2.2 nm). Additionally, DSC curves of opal-A 785 and 86.2 (Figure 4) display a major region of melting peaks near 0°C, suggesting that crystallizable water is enclosed in large pores (> 200 nm), resulting in a signal close to bulk conditions. None of the opal-CT samples have such bulk-like melting peak.

Sample	Onset temperature (°C)	Pore size (nm)	Sample	Onset temperature (°C)	Pore size (nm)
785	-5.7	4.54	**1552d**	-41.5	1.58
86.2	-5.6	4.60	**43l**	-23.2	1.95
1040	-13.5	2.55	**208**	-31.4	1.73
928	-18.1	2.18	**FT1111**	-36.2	1.65
1085	-32.1	1.72	**VTB**	-30.2	1.75
1545	-33.7	1.69	**WT86**	-41.0	1.59
1548	-25.36	1.88	**521**	-44.3	1.55
1543a	-37.61	1.63	**1551**	-38.1	1.62
1543b	-35.1	1.67	**YM12**	-48.1	1.52
1552b	-41.2	1.58			

Table 5: Onset temperature and calculated pore radii based on the DSC curves.

5.3.3 Pore size distribution (PSD)

In order to assess the microporosity filled with crystallizable water, we converted DSC curves into PSD according to the equation available in Landry (2005),slightly modified from Ishikiriyama and Todoki, 1995. For an efficient PSD, the baseline was based on the linear region of DSC curves. Parameters on each linear region of the DSC curves (before and after melting peak) were calculated. From the start of the melting peak (pointed manually), a coefficient was applied to weigh the contribution of each linear region. This coefficient is based on the portion of area for each point of the curves (and so, the proportion of solid that has melted) compared to the total area. The X-axis (temperature) is converted into pore radius according to the previously presented equation. The differential pore volume (dV/dr) is calculated according to:

$$\frac{dV}{dr} = \frac{dQ}{dt}\frac{dt}{d(\Delta T)}\frac{d(\Delta T)}{dr}\frac{1}{m\Delta H(T)\rho(T)}$$

Where *dQ/dt* is the measured heat flow, *d(ΔT)/dt* is the heating rate, *d(ΔT)/dr* is determined from the previous empirical equation, *m* is the dry mass of the material, *ΔH(T)* is the temperature-dependent heat of fusion of water (equation 25 from Landry (2005) and ρ(T) is the temperature-dependent density of ice (from Fukusako, 1990; Ishikiriyama and Todoki, 1995; Landry, 2005).

The average pore size and the full width at half maximum (FWHM) of the PSD are listed in Table 6. The average pore size calculated from PSD is consistent with those calculated from onset temperature, with a variation between 0.07 to 0.3 nm, except for samples 785 and 86.2, that display a difference of 2.08 nm. Given that water is used as probe liquid, we are not able to measure pores > 200 nm in radius (Landry, 2005). In consequence, opals with water close to bulk conditions (thus, opal 785 and 86.2 here) have a PSD excluding the existing big pores. This explains the differences between the average pore size calculated from onset temperature and from PSD. The FWHM differs from opal-A and –CT. Opal-A has a FWHM from 2.54 and 2.94 whereas opal-CT has FWHM from 0.34 to 1.39. Water-filled pore size appears to have a narrower distribution for opal-CT than opal-A. Even taking into account the limitations of measurements of thermoporosity using water (no pores greater than 200 nm can be measured), opal 785 and 86.2 have a larger distribution of PSD than opal-CT.

Sample	Average pore size (nm)	FWHM (nm)	Sample	Average pore size (nm)	FWHM (nm)
785	2.46	2.94	**1552d**	1.78	0.94
86.2	2.52	2.77	**43l**	2.06	0.96
1040	2.28	2.54	**208**	2	1.15
928	2.25	1.31	**FT1111**	1.88	0.78
1085	1.89	0.7	**VTB**	2.05	0.9
1545	1.86	1.15	**WT86**	1.78	0.76
1548	1.81	1.39	**521**	1.72	0.34
1543a	1.82	1.04	**1551**	1.83	0.97
1543b	1.82	1.15	**YM12**	1.69	0.46
1552b	1.74	0.79			

Table 6: Average pore size and full width at half maximum calculated from the PSD.

5.4 Raman Spectroscopy

Eight samples were investigated under Raman spectroscopy. Among the eight samples, 2 main behaviours were identified. Raman signatures and observations with cross-polar differ between fresh and old samples.

5.4.1 Cracking of fresh samples

Among the 5 fresh samples, 3 of them cracked during heating, while KOK01 and AN02 appear to resist. Interestingly, KOK01 and AN02 are the only fresh hydrophane samples. Except for CH01, the reference piece of each sample did not crack after 2 months. All samples cracked during the heating ramp to 150°C. After cracking, samples were examined at room temperature, between cross polar, and a strong anisotropy located around the cracks was observed (whereas before cracking, samples were totally isotropic: Figure 5 below).

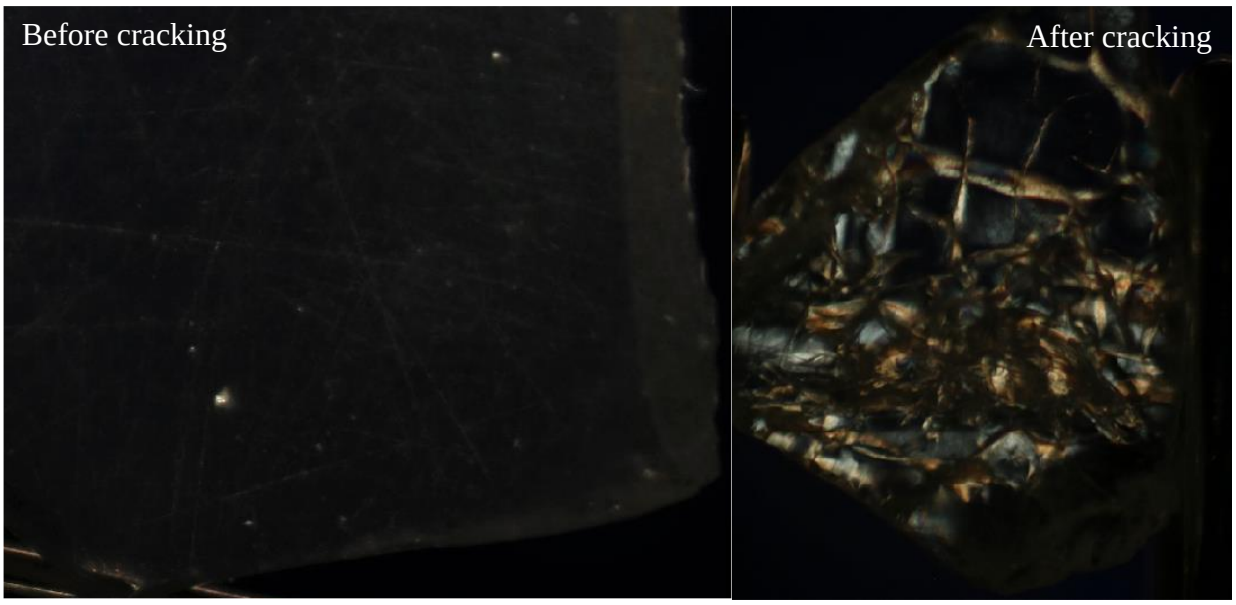

Figure 5: Microphotographs between cross-polar of KOK04 sample before and after cracking by heating.

On these samples, and for each heating step, 256 spectra were acquired following a grid 16x16 with 10µm spacing. A map of variations of the position of each band can be extrapolated. However, the high noise level prevents effective use of this technique. Nevertheless, we can assess the total variation efficiently using the large number of spectra acquired. Thus, an average spectrum at room temperature (before cracking) and at 150°C (after cracking) has been calculated to emphasize the variation.

The 3 samples exhibiting a strong cracking at 150°C also show variations in the position of the Raman bands (Raman modes defined in Etchepare et al., 1978 and Ostrooumov et al., 1999). Bands shift from 3 to 14 cm^{-1} according to the sample and the bands. All bands shift toward lower frequencies.

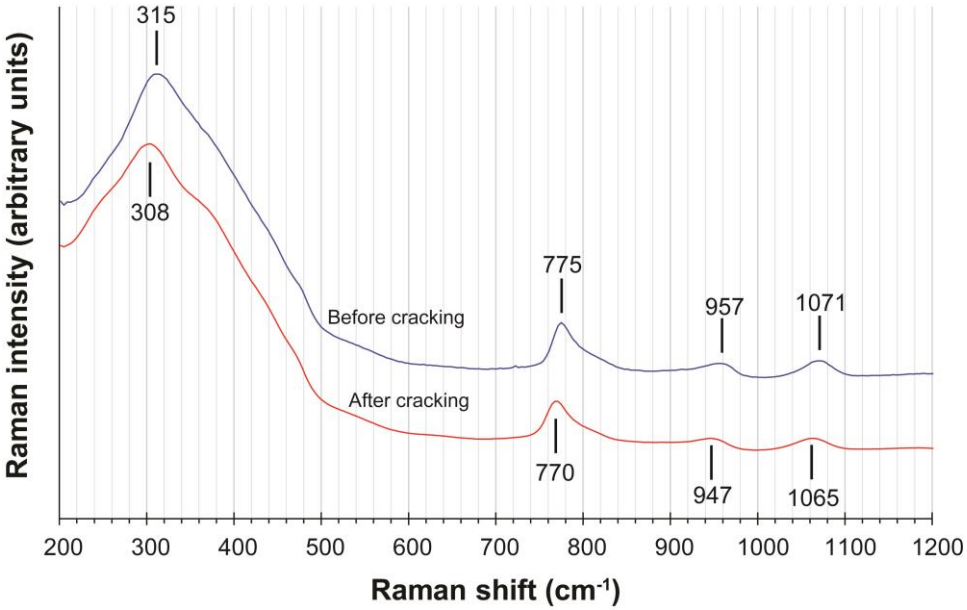

Figure 6: Raman spectra before and after cracking of KOK04.

5.4.2 Cracking of old samples

Old samples analysed here (1548, 1552a, 1543b) crack near 300°C (Table 2). For these samples, the cracking does not induce any anisotropic features between cross-polar. Before and after cracking, samples remain totally isotropic.

As with the fresh samples, we acquired maps of Raman spectra (with a minimum of 200 spectra following several grids with a spacing of 75 to 150 µm) to observe possible variations. However, at room temperature, 150°C or 300°C, with a resolution of 0.8 cm^{-1}, no variations in the position of Raman bands were emphasized (Figure 7).

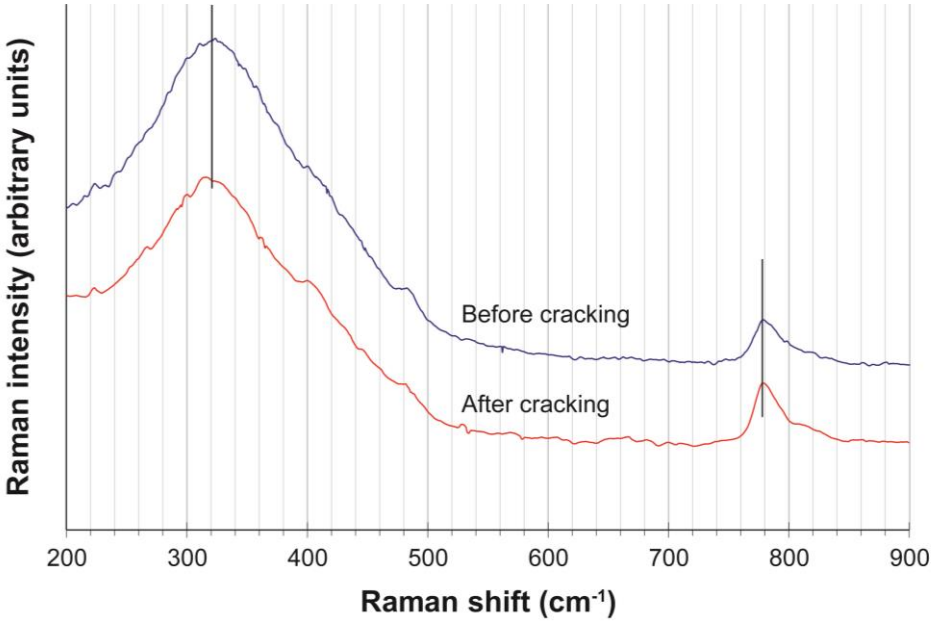

Figure 7: Raman spectra of 1548 before and after cracking.

6. DISCUSSION

6.1 Incorporation of water in opal

6.1.1 Water speciation

The major role played by water in opal formation results in a wide range of water content in opal (from 1 to 15 wt%; Brown et al., 2002; Day and Jones, 2008; Jones and Segnit, 1969; Langer and Flörke, 1974; Thomas et al., 2010). Water has been shown to exist in molecular form (trapped in silica cages) and silanol groups (Si-OH) in opal (Langer & Flörke, 1974a; Graetsch et al., 1985; Boboň et al., 2011; Chauviré et al., 2017a). Near Infrared and NMR spectroscopy has indicated that most of the water is molecular (Langer & Flörke, 1974a; Brown et al., 2002; Chauviré et al., 2017a). Most studies affirm that molecular water is present in interstices between spheres (Jones & Segnit, 1969; Langer & Flörke, 1974a), whereas recent work demonstrates that water is enclosed in smaller pores (Smallwood et al., 2008b). The mobility of water in opal is brought forward in the study of the destabilization of gem opal (cracking and whitening; Pearson, 1985; Rondeau et al., 2011).

By combining DSC measurements of crystallisable water content and TGA, we estimate the proportion of crystallisable water compared to total water (outlined in Table 3 and **Error! Reference source not found.**, results in Table 7). Therefore, 3.1 to 45.7 % of water contained in the opals analysed consists in crystallizable molecular water. Our analysis significantly widens the range identified in Thomas et al. (2013) (from 6.3 to 22.2 %). The proportion of crystallisable water in opal appears to be independent of the structure of opal; opal-A has a percentage of crystallisable water ranging from 13.3 to 20.7 % and in opal-CT, this ranges between 3.1 to 45.7 %. Note that opal-A has a proportion of crystallisable water with a narrower range (from 6 to 21 % by taking account of the analyses from Thomas et al. (2013)) than opal-CT (from 3.1 to 45.7 %). In fact, in opal, up to 45 % of the molecular water (or 4 % of the total water content) is mobile and may be lost during dehydration under ambient conditions (*modulo* the connected porosity), an important factor for the investigation of opal destabilization.

Sample	Proportion of crystallizable water (%)	Sample	Proportion of crystallizable water (%)
785	13.6	**1552d**	28.9
86.2	20.7	**43l**	3.1
1040	13.1	**208**	19.7
928	10.4	**FT1111**	7.2
1085	25.0	**VTB**	5.4
1545	31.8	**WT86**	27.7
1548	45.7	**521**	5.2
1543a	34.3	**1551**	18.9
1543b	39.6	**YM12**	9.1
1552b	25.1		

Table 7: Proportion of crystallisable water relatively to the total water content.

6.1.2 Water-filled porosity

Water molecules in opals are assumed mainly to be integrated between large spheres (several hundreds of nanometres), and to constitute a major part (> 80%) of the total water content (Langer & Flörke, 1974b; Brown et al., 2003; Smallwood et al., 2008a). Our analysis demonstrated that most of the crystallizable water (up to 50% of the total water content) is contained in nanometric pores. Considering the idealized view of opal, with an arrangement of silica spheres of similar size in a cubic or hexagonal packing, the voids between large spheres measure between several nanometres and several hundred nanometres. However, this idealized view, and most microphotographs of opal microstructure (done after etching with hydrofluoric acid), neglect the silica that cements the spheres. Even if large cavities may be filled by water, as observed in 2 opal-A here, it appears that most of the water is enclosed in nanometric pores, which underlines the significant role of cement in the incorporation of water.

Additionally, at a smaller scale, opal is constituted of nanograins from 10 to 50 nm, composing the larger microstructural units (spheres or lepispheres, fibres, platelets; Gaillou et al., 2008). Spaces between nanograins is consistent with nanometric pores. Therefore, in contrast with the commonly-used model for water incorporation in opal from earlier studies (Jones & Segnit, 1969; Langer & Flörke, 1974a; Graetsch et al., 1994), molecular water may be enclosed in voids between nanograins, inside microstructural units.

The PSD of our sample shows that opal-CT contains water in smaller pores than opal-A, with a narrower distribution. Firstly, smaller pores measured in opal-CT may be explained geometrically. In fact, nanograins in opal-CT may arrange in several types of microstructural units, but never in perfect spheres allowing the largest kind of cavity (seen in opal-A). Second, the narrower distribution suggests that opal-CT have nanograins with limited sizes compared to opal-A. Alternatively, given that the spheres composing opal-A allow the creation of large cavities, larger pores will add to the distribution from the arrangement of nanograins, and thus widen the distribution of pore sizes.

The readers must bear in mind that thermoporosimetry assesses only the pores filled with water (or any other probe liquid), and that it cannot measure empty pores. Consequently, opal-CT may have large pores, but either molecular water does not penetrate them, or these porosities have lost their water. However, large pores in opal-A retain the water. In all cases, our study demonstrates that water retained in opal is present in nanometric pores.

6.2 Reactions during heating dehydration

Three kinds of dehydration were identified with TGA (sample with a plateau before dehydration, quick dehydration, progressive dehydration). These behaviours are consistent with the infrared spectroscopy heating experiments from Chauviré (2015). The combination of these analyses demonstrate that the dehydration mainly concerns the loss of molecular water. Indeed, as studied by Thomas et al. (2015), silanols required higher temperatures to be released.

Moreover, the temperatures of cracking in opals showing a plateau in TGA are generally consistent with the end the plateau. We noticed that most of the sample react (cracking or whitening) at around 300°C. Therefore, it appears that a high temperature is required to induce cracking in these samples. Samples 928 and 1545 showing a plateau do not crack, and 785 and 86.2 whiten at this temperature. Samples that dehydrate mainly at low temperatures (< 300°C) either whiten at high temperatures

(over 300°C) or resist (except for 521 that cracks at 300°C). The remaining samples (1551 and 43l) that lose their water progressively whiten at high temperatures (over 500°C).

A significant difference has been identified between the old samples and the fresh ones. Indeed, during the cracking, fresh samples (cracking at low temperatures) show a development of constrains inside the silica. By contrast, old sample do show any constrains, even after cracking (at higher temperature). Thus, old samples do not record the constrains during cracking, suggesting that the process is only induced at high temperatures, and not present at low temperatures. Unlike the fresh samples that crack at their first exposure to the atmosphere, old samples required high temperatures in order to react.

6.3 Cracking origin?

To crack, a material has to be exposed to a constrain greater than it can resist. The cracking resistance of a material may be calculated using several methods. On natural opal, only one study has measured the parameters required to estimate this resistance (Thomas et al., 2008). However, several studies have investigated the propagation of cracks in amorphous silica (e.g. Rimsza et al., 2018). The propagation of cracks, according to the Linear Elastic Fracture Mechanism, is related to the elastic modulus of the material (measured on natural opal by Thomas et al., 2008), the length of the initial cracks, and the bond energy. The greater the crack length, the lower the stress required to propagate the cracks. If we assume that opal does not present visible cracks before destabilization, it appears that the initial state is composed of cracks smaller than 1 micron. In these cases, the stress required to propagate cracks has to be greater than 400 MPa for micrometric cracks, and up to 13.5 GPa for nanometric cracks. The 2 main models that explain cracking may be given.

6.3.1 Internal water pressure

As far as the internal pressure induced by fluids is concerned, the liquid had to be included in a closed porosity, as an open porosity releases the pressure. The first assumption - that the vapour pressure in the ground may be involved - may be not valid. Indeed, the vapour pressure in the ground never reaches a pressure greater than the cracking pressure.

Samples presenting TGA curves with a plateau under 300°C obviously contain water in closed porosity (otherwise, the water could be released under 300°C), so this process could be involved in their cracking. The pressure induced by fluid inside a porosity is related to the temperature, the thermal expansion (α) and the compressibility (β) of the fluid (Swain, 1981; Dutrow & Norton, 1995) :

$$\frac{\partial P}{\partial T} = \frac{\alpha}{\beta}$$

For water, the pressure induced by heating these fluids reaches up to 450 MPa at 300°C, and 600 MPa at 400°C (data from Johnson and Norton, 1991). After the critical point of water (where water is in critical state), the pressure induced drastically decreases. Therefore, it is not surprising that, for samples with water in closed porosities, cracking occurs at high temperatures, but lower than the critical point (from 623 K to 647 K depending on pore size, Hiejima and Yao, 2004). Moreover, for these samples, the stress induced by the expansion of fluid in the porosity is entirely released after cracking, and this is consistent with the observations between cross-polars and by Raman

spectroscopy. Interestingly, the DSC data show that these samples also have a significant proportion of free water. The expansion of water may also explain the increase of volume measured by thermomechanical analysis on Australian opal by Brown et al. (2002) and Thomas et al. (2010).

6.3.2 Drying shrinkage

The second model is the drying shrinkage of silica during the loss of water. This process occurs if the water enclosed in porosity is released and induces capillary pressure on the silica framework. The stress involved may also be modelled (Brinker & Scherer, 1990; Smith et al., 1995; Scherer, 1997). The model is based on the hydrophility of the solid (here, the amorphous silica), defined by the contact angle between water and silica (θ), the bond energy of water between the liquid and the vapour phase (γ_{LV}), and the characteristic of the porosity (density of the bulk material -ρ_b-, and the relative density –ρ-, as well as the surface area - S).

$$P = \gamma_{LV} \cos(\theta) \left(\frac{S \rho_b}{1 - \rho} \right)$$

We may simplify this equation if we assume a shape for the pores (spherical, cylindrical …). If we assume cylindrical pores, for water in pores smaller than 10 nm (as calculated here), the capillary pressure is greater than 2000 MPa (up to 22 GPa in pores of 1 nm ; from Smith et al., 1995). However, in this calculation, the entire porosity is assumed to be filled with water, and our data only estimates the filled porosity (because of the absence of the gas adsorption analysis).

This model explains well the cracking in fresh samples, at room temperature, or “low” temperatures (less than 200°). Moreover, the process induces stress even after cracking, consistent with the examinations between cross-polars or Raman analysis.

7. CONCLUSION

In this project, we investigated the incorporation of water in opal and the behaviour of silica during dehydration. Novel data from DSC analysis demonstrates that opal may contain almost half of its water as free water, and that most of this water is enclosed in nanometric pores (either between large spheres or nanograins). We underline that destabilization of opal is different if the sample is fresh (extracted recently and preserved in water) or old (extracted several years ago and preserved in the atmosphere). Indeed, the old samples appear to crack only if we apply a high temperature (more than 300°C), probably due to an internal pressure induced by the temperature. In these cases, these samples appear to be stable over time, as long as they are not exposed to high temperature.

For fresh samples, it appears that our data are consistent with a drying shrinkage. Thus, cracking occurs when the capillary pressure induced during the loss of water is greater than the resistance of the material. In these cases, several factors control the pressure. On opals, we probably cannot change the porosity characteristics of the materials, but we may influence the hydrophility of the material and the bond energy (more details in 6.3.2). Indeed, as described for silica gel drying, we may add surfactant to increase the contact angle, and thus decrease the capillary pressure. We may also avoid the bond energy by suppressing it by drying opal in the critical conditions (Brinker & Scherer, 1990).

Our data does not provide significant information about the whitening. Indeed, during the drying of a gel, several studies observe similar features as in natural opal – a ring of opaque material circling a more translucent core (Hench & Wilson, 1990; Scherer, 1992b). The opacity is explained by the transition zone between dry and wet material. In this area, pores filled with water mix with dry pores. The difference in the optic characteristics between the two areas induces light scattering. However, on opal, more analysis is required in order to reach any conclusions.

Further analysis is required to create an efficient diagnostic protocol for destabilization. First, the resistance of the material needs to be accurately estimated. Only one study measures mechanical parameters on natural opals, and it is restricted to Australian opal-A (Thomas et al., 2008). Nanoidentitation analysis on a large and comprehensive set of opal is needed to better estimate the resistance of the material. Moreover, the measurement of the total porosity on each sample (perhaps by X ray nanotomography) is required to test whether cracking follows the drying shrinkage equation established on silica gel. In addition, we need to collect more samples directly in the field, to monitor the destabilization in real time, and have actual access to the process without forced dehydration. Indeed, we demonstrate here that heating may induce a different process than the natural process.

The project has provided significant data towards a fuller understanding of the destabilization of opal, and has explored new ways of characterizing the factors responsible for the instability.

8. REFERENCES

Aguilar-Reyes, B. (2004): Etude microstructurale des opales : application à la déstabilisation par blanchissement. *Thèse Dr.* Université de Nantes.

Boboň, M., Christy, A.A., Kluvanec, D., & Illášová, L. (2011): State of water molecules and silanol groups in opal minerals: a near infrared spectroscopic study of opals from Slovakia. *Phys. Chem. Miner.*, **38**, 809–818.

Born, M., Wolf, E., Bhatia, A.B., Clemmow, P.C., Gabor, D., Stokes, A.R., Taylor, A.M., Wayman, P.A., & Wilcock, W.L. (1999): Principles of Optics. Cambridge University Press, Cambridge.

Brinker, C.J., & Scherer, G.W. (1990): Sol-Gel Science - The Physics and Chemistry of Sol-Gel-Processing, 908 p.

Brown, L.D., Ray, A.S., Thomas, P.S., & Guerbois, J.P. (2002): Thermal characteristics of Australian sedimentary opals. *J. Therm. Anal. Calorim.*, **68**, 31–36.

Brown, L.D., Ray, A.S., & Thomas, P.S. (2003): 29Si and 27Al NMR study of amorphous and paracrystalline opals from Australia. *J. Non. Cryst. Solids*, **332**, 242–248.

Brun, M., Lallemand, A., Quinson, J.-F., & Eyraud, C. (1977): A new method for the simultaneous determination of the size and shape of pores: the thermoporometry. *Thermochim. Acta*, **21**, 59–88.

Cassedanne, J.-P.O., & Cassedanne, J.-P.O. (1975): L'opale verte de la Fazenda Brejinho (Brésil). *Bull. l'A.F.G.*, **45**, 6–7.

Chauviré, B. (2015): Genèse de silice supergène sur Terre et implications sur Mars. University of Nantes, Ecole Centrale de Nantes.

Chauviré, B., Rondeau, B., & Mangold, N. (2017a): Near infrared signature of opal and chalcedony as a proxy for their structure and formation conditions. *Eur. J. Mineral.*, **29**, 409–421.

Chauviré, B., Rondeau, B., Mazzero, F., & Ayalew, D. (2017b): The Precious Opal Deposit At Wegel Tena, Ethiopia: Formation Via Successive Pedogenesis Events. *Can. Mineral.*, **55**, 701–723.

Darragh, P.J., & Sanders, J. V (1965): The origin of colour in opal. *Aust. Gemol.*, **7**, 9–12.

Darragh, P.J., Gaskin, A.J., & Sanders, J. V. (1976): Opals. *Sci. Am.*, **234**, 84–95.

Day, R., & Jones, B. (2008): Variations in Water Content in Opal-A and Opal-CT from Geyser Discharge Aprons. *J. Sediment. Res.*, **78**, 301–315.

Des Cloizeaux, A. (1862): Manuel de Minéralogie, 572 p. (Dunod, Ed.). Paris.

Dutrow, B., & Norton, D. (1995): Evolution of fluid pressure and fracture propagation during contact metamorphism. *J. Metamorph. Geol.*, **13**, 677–686.

Etchepare, J., Merian, M., & Kaplan, P. (1978): Vibrational normal modes of SiO2. II. Cristobalite and tridymite. *J. Chem. Phys.*, **68**, 1531.

Frischat, G.H., Schwander, R., Beier, W., & Weeks, R.A. (1989): High-temperature thermal expansion of libyan desert glass as compared to that of silica glasses and natural silicates. *Geochim. Cosmochim. Acta*, **53**, 2731–2733.

Fritsch, E., Rondeau, B., Ostroumov, M., Lasnier, B., Marie, A.-M., Barrault, A., Wery, J., Connoué, J., & Lefrant, S. (1999): Découvertes récentes sur l'opale. *Rev. Gemol. A.F.G.*, **138/139**, 34–40.

Fukusako, S. (1990): Thermophysical properties of ice, snow, and sea ice. *Int. J. Thermophys.*, **11**, 353–372.

Gaillou, E., Fritsch, E., Aguilar-Reyes, B., Rondeau, B., Post, J., Barreau, A., & Ostroumov, M. (2008): Common gem opal: An investigation of micro- to nano-structure. *Am. Mineral.*, **93**, 1865–1873.

Gauthier, J.-P., Mazzero, F., Mandaba, Y., & Fritsch, E. (2004): L'opale d'Ethiopie : gemmologie ordinaire et caractèristiques exceptionnelles. *Rev. Gemol. A.F.G.*, **149**, 15–23.

Graetsch, H., Flörke, O.W., & Miehe, G. (1985): The nature of water in chalcedony and opal-C from brazilian agate geodes. *Phys. Chem. Miner.*, **12**, 300–306.

Graetsch, H., Gies, H., & Topalović, I. (1994): NMR, XRD and IR study on microcrystalline opals. *Phys. Chem. Miner.*, **21**, 166–175.

Hansteen, T.H., & Klugel, A. (2008): Fluid Inclusion Thermobarometry as a Tracer for Magmatic Processes. *Rev. Mineral. Geochemistry*, **69**, 143–177.

Hench, L. (1998): Sol- Gel Kinetics, Noyes Publ., 168 p.

Hench, L.L., & Wilson, M.J.R. (1990): Processing of gel-silica monoliths for optics. Drying behavior of small pore gels. *J. Non. Cryst. Solids*, **121**, 234–243.

Hiejima, Y., & Yao, M. (2004): Phase behaviour of water confined in Vycor glass at high temperatures and pressures. *J. Phys. Condens. Matter*, **16**, 7903–7908.

Iler, R.K. (1979): The Occurrence, Dissolution, and Deposition of Silica. In J.W. and Sons, Ed., *Chem. Silica Solubility, Polym. Colloid Surf. Prop. Biochem. Silica* pp. 3–93. New York.

Ishikiriyama, K., & Todoki, M. (1995): Pore Size Distribution Measurements of Silica Gels by Means of Differential Scanning Calorimetry. *J. Colloid Interface Sci.*, **171**, 103–111.

Johnson, J.W., & Norton, D. (1991): Critical phenomena in hydrothermal systems: state, thermodynamic, electrostatic, and transport properties of H2O in the critical region. *Am. J. Sci.*, **291**, 541–648.

Johnson, M.L., Kammerling, R.C., Deghionno, D.G., & Koivula, J.I. (1996): Opal from Shewa province, Ethiopia. *Gems Gemol.*, **32**, 112–120.

Jones, J.B., & Segnit, E.R. (1969): Water in Sphere-Type Opal. *Mineral. Mag.*, **37**, 357–361.

Jones, J.B., Sanders, J. V., & Segnit, E.R. (1964): Structure of Opal. *Nature*, **204**, 990–991.

Kistler, S.S. (1931): Coherent Expanded-Aerogels. *J. Phys. Chem.*, **36**, 52–64.

Lacroix, A. (1896): Minéralogie de la France, 804 p. Paris.

Landry, M.R. (2005): Thermoporometry by differential scanning calorimetry: Experimental considerations and applications. *Thermochim. Acta*, **433**, 27–50.

Langer, K., & Flörke, O.W. (1974a): Near infrared absorption spectra (4000-9000 cm-1) of opals and the role of "water" in these SiO2-nH2O minerals. *Fortschritte der Mineral.*, **52**, 17–51.

——— (1974b): Near infrared absorption spectra (4000–9000 cm- 1) of opals and the role of "water" in these SiO 2· nH 2 O minerals. *Fortschritte der Mineral.*, **52**, 17–51.

Lockwood, D.J. (2015): Rayleigh and Mie Scattering. In R. Luo, Ed., *Encycl. Color Sci. Technol.* pp. 1–12. Springer New York, New York, NY.

Malchow, P., Johanns, K.E., Möncke, D., Korte-Kerzel, S., Wondraczek, L., & Durst, K. (2015): Composition and cooling-rate dependence of plastic deformation, densification, and cracking in sodium borosilicate glasses during pyramidal indentation. *J. Non. Cryst. Solids*, **419**, 97–109.

Mollé, V. (2017): Caractérisation de la déstabilisation de l'opale par fissuration.

Ostrooumov, M., Fritsch, E., Lasnier, B., & Lefrant, S. (1999): Spectres Raman des opales: aspect diagnostique et aide à la classification. *Eur. J. Mineral.*, **11**, 899–908.

Paris, M., Fritsch, E., & Aguilar-Reyes, B. (2007): 1H, 29Si and 27Al NMR study of the destabilization process of a paracrystalline opal from Mexico. *J. Non. Cryst. Solids*, **353**, 1650–1656.

Pearson, G. (1985): Role of Water in Cracking of Opal. *Aust. Gemol.*, **15**, 435–445.

Perriot, A., Vandembroucq, D., Barthel, E., Martinez, V., Grosvalet, L., Martinet, C., & Champagnon, B. (2006): Raman Microspectroscopic Characterization of Amorphous Silica Plastic Behavior. *J. Am. Ceram. Soc.*, **89**, 596–601.

Phalippou, J., Woignier, T., & Prassas, M. (1990): Glasses from aerogels. *J. Mater. Sci.*, **25**, 3111–3117.

Rimsza, J.M., Jones, R.E., & Criscenti, L.J. (2018): Crack propagation in silica from reactive classical molecular dynamics simulations. *J. Am. Ceram. Soc.*, **101**, 1488–1499.

Rondeau, B., Fritsch, E., Mazzero, F., & Gauthier, J. (2011): Opal – The Craze for Stability. *Color*, **Winter**, 2–5.

Scherer, G.W. (1992a): Crack-tip stress in gels. *J. Non. Cryst. Solids*, **144**, 210–216.

——— (1992b): Recent progress in drying of gels. *J. Non. Cryst. Solids*, **147**–**148**, 363–374.

——— (1997): Effect of drying on properties of silica gel. *J. Non. Cryst. Solids*, **215**, 155–168.

Smallwood, A.G., Thomas, P.S., & Ray, A.S. (2008a): Comparative analysis of sedimentary and volcanic precious opals from Australia. *J. Aust. Ceram. Soc.*, **44**, 17–22.

——— (2008b): The thermophysical properties of australian opal. In *Proc. 9th Int. Congr. Appl. Mineral.* pp. 557–565. Bisbane, Queensland.

Smith, D.M., Scherer, G.W., & Anderson, J.M. (1995): Shrinkage during drying of silica gel. *J. Non. Cryst. Solids*, **188**, 191–206.

Smith, K.L. (1988): Opals from Opal Butte, Oregon. *Gems Gemol.*, **24**, 229–236.

Swain, M. V. (1981): Nickel sulphide inclusions in glass: an example of microcracking induced by a volumetric expanding phase change. *J. Mater. Sci.*, **16**, 151–158.

Tallant, D.R., Michalske, T.A., & Smith, W.L. (1988): The effects of tensile stress on the Raman spectrum of silica glass. *J. Non. Cryst. Solids*, **106**, 380–383.

Thiery, J., Keita, E., Rodts, S., Courtier Murias, D., Kodger, T., Pegoraro, A., & Coussot, P. (2016): Drying kinetics of deformable and cracking nano-porous gels. *Eur. Phys. J. E*, **39**.

Thomas, P.S., Smallwood, A.S., Ray, A.S., Briscoe, B.J., & Parsonage, D. (2008): Nanoindentation hardness of banded Australian sedimentary opal. *J. Phys. D. Appl. Phys.*, **41**, 074028.

Thomas, P.S., Šesták, J., Heide, K., Fueglein, E., & Šimon, P. (2010): Thermal properties of Australian sedimentary opals and Czech moldavites. *J. Therm. Anal. Calorim.*, **99**, 861–867.

Thomas, P.S., Guerbois, J.-P., & Smallwood, A.G. (2013): Low temperature DSC characterisation of water in opal. *J. Therm. Anal. Calorim.*, **113**, 1255–1260.

Thomas, P.S., Heide, K., & Földvari, M. (2015): Water and hydrogen release from perlites and opal. *J. Therm. Anal. Calorim.*, **120**, 95–101.

Vityk, M.O., & Bodnar, R.J. (1995): Textural evolution of synthetic fluid inclusions in quartz during reequilibration, with applications to tectonic reconstruction. *Contrib. to Mineral. Petrol.*, **121**, 309–323.

Wanamaker, B.J., Wong, T.-F., & Evans, B. (1990): Decrepitation and crack healing of fluid inclusions in San Carlos olivine. *J. Geophys. Res.*, **95**, 15623.

Zarzycki, J., Prassas, M., & Phalippou, J. (1982): Synthesis of glasses from gels: the problem of monolithic gels. *J. Mater. Sci.*, **17**, 3371–3379.